Electronic Supplementary Information

Flat-plate mesophotoreactor with the serpentine channel and inclined baffles for balancing mixing performance and reaction throughput

Shuaiyu Chen[a,‡], *Qianrui Lv*[b,‡], *Fujun Li*[a], *Yuchao Wang*[a], *Wenbo Yang*[a], *Alexander A. Miskevich*[c], *Valery A. Loiko*[c], *Shengyang Tao*[a], *Lijing Zhang*[a,*]

[a] School of Chemistry, State Key Laboratory of Fine Chemicals, Frontier Science Center for Smart Materials, Dalian Key Laboratory of Intelligent Chemistry, Dalian University of Technology, Dalian 116024, China.

[b]School of Science, Beijing Jiaotong University, Beijing 100044, China.

[c]Institute of Physics, National Academy of Sciences of Belarus, 68-2 Niezalezhnastsi ave., Minsk, 220072, Belarus

* Corresponding author: Lijing Zhang

E-mail address: zhanglj@dlut.edu.cn

Simulation Section

1. Optimization of mesoscopic reactor structures

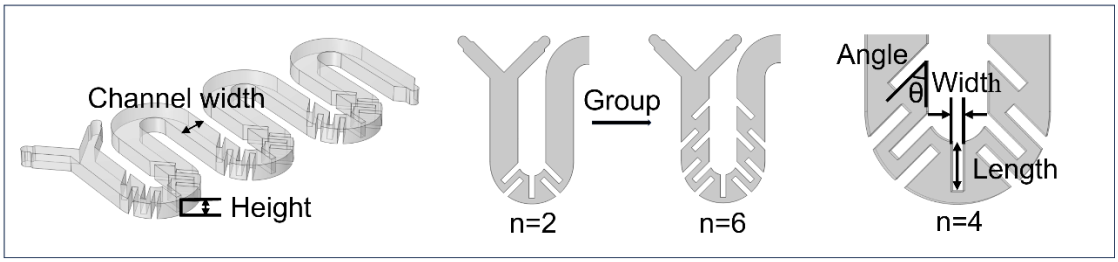

The initial parameters of the reactor are as follows: channel width is 5 mm, with 4 groups of baffles placed, each baffle being 4 mm in length and 1 mm in width, and the reactor height is 1 mm. The optimized baffle parameters include groups of 2, 3, 4, 5, and 6, with lengths of 3.5, 4, and 4.5 mm, widths of 0.8, 1, and 1.2 mm, angles of 40°, 45°, and 50°, and reactor heights of 1, 3, and 5 mm. After determining the optimal grid through the mesh independence test, the mixing index and pressure drop were used as optimization parameters to optimize the number of baffle placement groups, length, width, angle, and reactor height. First, the number of baffle placement groups in the reactor was optimized and a flow rate range of 0.1-5 mL/min was selected. As shown in Fig. S1a, the mixing index increases with the number of groups. At flow rates greater than 1 mL/min, the mixing indexes for reactors with different numbers of baffle groups are higher than 0.9. However, when the flow rate exceeds 1.5 mL/min and the number of baffle groups is four or more, complete mixing is only achieved and maintained stably. As seen in Fig. S1b, the pressure drop increases with the number of groups. When the number of baffle groups is greater than 4, the mixing effect no longer changes, only resulting in a continuous rise in pressure drop. Therefore, after comprehensive consideration, the optimized number of baffle groups is 4.

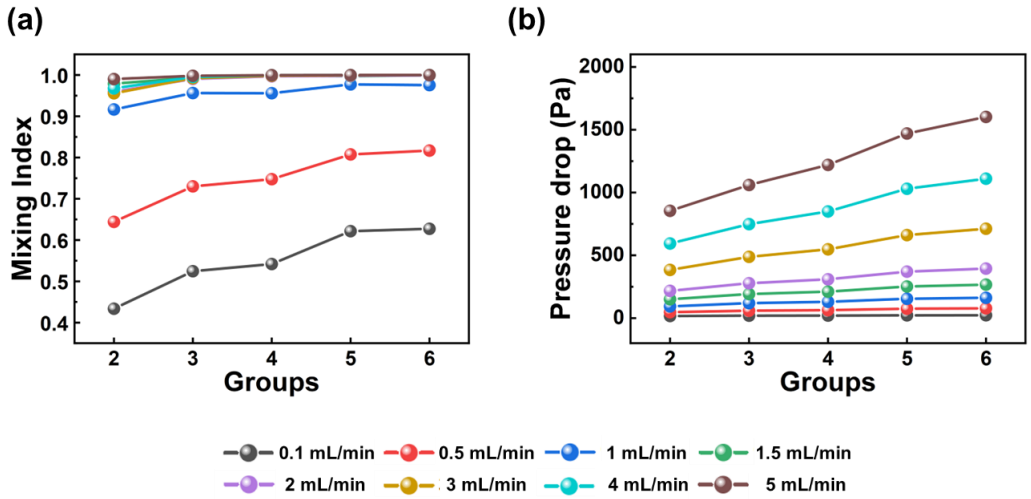

Fig. S1 (a) Variation of mixing index with the number of baffle placement groups. (b) Variation of pressure drop with the number of baffle placement groups.

Next, the geometric parameters of the baffles were optimized, starting with the baffle length. As shown in Fig. S2a, the mixing index increases with the baffle length across all flow rates. When the flow rate exceeds 1.5 mL/min, the mixing index is nearly 1 with a baffle length of 4 mm and doesn't increase further with additional length. However, from Fig. S2b, it can be found that the pressure drop increases with the increase of baffle length, while the increase of pressure drop is more than doubled when the baffle length is extended from 4 mm to 4.5 mm. Therefore, after comprehensive consideration, the optimized baffle length is 4 mm. Consequently, the width of the baffle was optimized. The effect of width on the mixing index and pressure drop is similar to that of length. As indicated by Fig. S2c and d, the flow rate above 1.5 mL/min tends to mix completely. At 1 mL/min, there is a slight improvement when comparing 1 mm to 0.8 mm, while the increase in pressure drop is not obvious. However, when the width is increased from 1 mm to 1.2 mm, the mixing index remains almost unchanged, with only a slight rise in pressure drop. After comprehensive consideration, 1 mm was selected as the optimal baffle width. Finally, the placement angle of the baffles was optimized. As shown in Fig. S2e and f, the mixing index levels off at flow rates above 1 mL/min, and the pressure drop is the lowest across the selected flow range when the baffle angle is set at 45°. Hence, the baffle inclination angle was set at 45°.

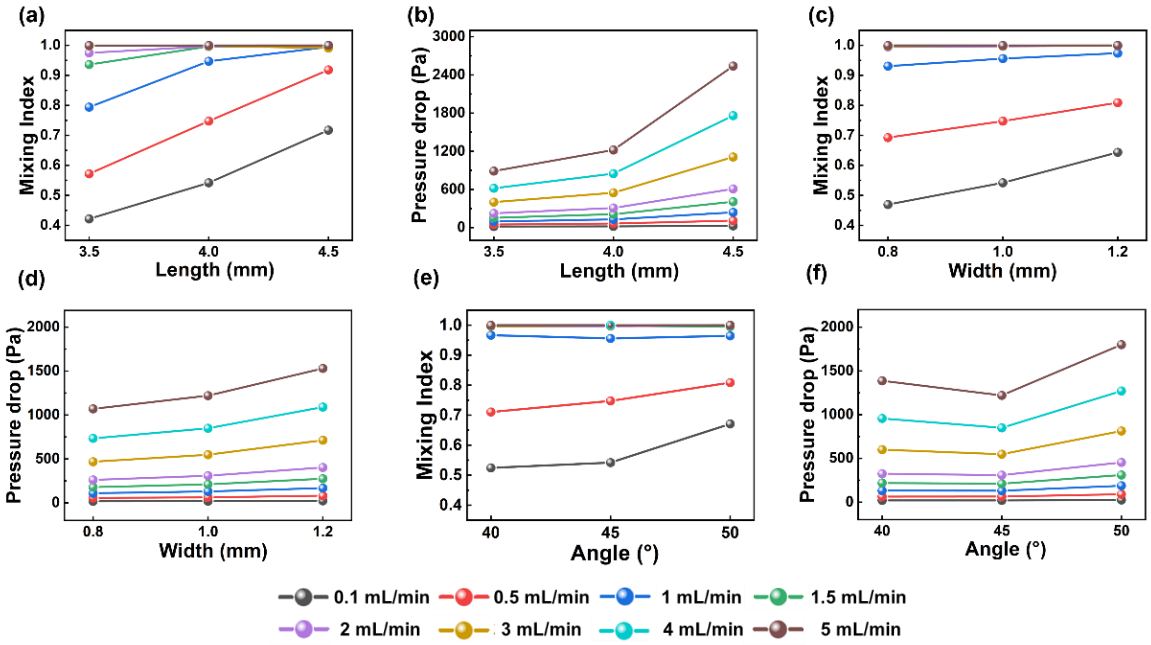

Fig. S2 (a) Variation of mixing index with baffle length. (c) Variation of mixing index with baffle width. (e) Variation of mixing index with baffle angle. (b) Variation of pressure drop with baffle length. (d) Variation of pressure drop with baffle width. (f) Variation of pressure drop with baffle angle.

Finally, the height of the reactor was optimized. As can be inferred from Fig. S3a and b, when the reactor height is increased from 1 mm to 3 mm, and the flow rate ranges from 0.5 to 1.5 mL/min, the mixing index decreases significantly with the increase in channel height. However, at a flow rate of 0.1 mL/min, on the contrary, the mixing index tends to increase with the channel height. Next, this phenomenon is analyzed. According to eqn (1), when molecular diffusion dominates the intermolecular interaction, the larger the height-to-width aspect ratio of the reactor, the greater the molecular contact area, and the shorter the distance required for complete mixing[1]. Since mixing at a flow rate of 0.1 mL/min relies on molecular diffusion, when the reactor height increases, the larger molecular contact area results in better mixing, causing the mixing index to increase with the reactor height. When the flow rate is above 2 mL/min, the mixing effect hardly changes and still tends towards complete mixing. However, when the height is further increased to 5 mm and the flow rate is above 2 mL/min, the mixing index will also decrease sharply, even falling below 0.8. The pressure drop significantly decreases when the height is increased from 1 mm to 3 mm, but it hardly changes when further increased to 5 mm. Therefore, considering all factors, 3 mm was chosen as the optimal height.

The minimum length L_m of the channel for complete mixing is defined as follows:

$$L_m = \frac{Q}{8\alpha D} \quad (1)$$

Where Q is the flow rate at each inlet, α is the height-to-width aspect ratio of a reactor, and D is the diffusion coefficient.

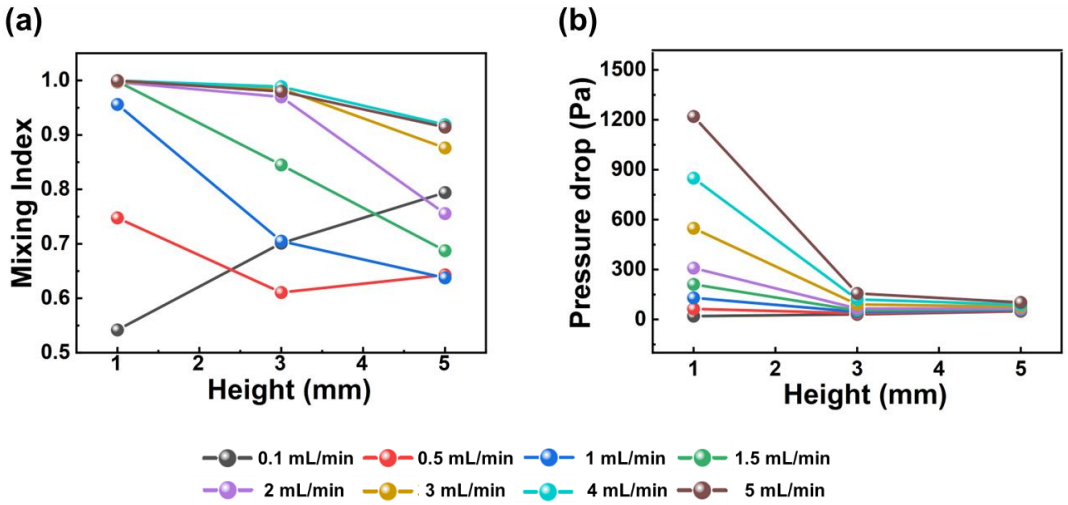

Fig. S3 (a) Variation of mixing index with reactor height. (b) Variation of pressure drop with reactor height.

2. Velocity distribution of M_3 in y and z directions

To investigate the velocity distribution characteristics of fluids in a curved channel space, the velocity distribution in the *y*-direction from the top of the baffle to the channel sidewall was extracted. Fig. S4a shows the *y*-values and their corresponding position coordinates. The coordinate of the top of the baffle is (7.5, 0, 1.5), and the reactor boundary coordinate is (7.5, 1000, 1.5). The corresponding velocity distribution is shown in Fig. S4b. It can be observed that when the flow rate is 0.5 mL/min, the velocity at the top of the baffle gradually increases, reaching a peak at a distance of 480 μm from the top. As the distance increases further, the fluid velocity gradually decays, approaching zero on the wall surface. When the fluid enters the reactor at different flow rates, the overall trend of velocity in the *y*-direction is the same, but the position where the maximum velocity occurs changes slightly. The flow rates of 2 mL/min and 5 mL/min correspond to velocity peaks at distances of 560 μm and 600 μm from the top of the baffle, respectively. The variation in the position of the maximum velocity in the *y*-direction with flow rate indicates that as the flow rate rises, the distance of fluid flow direction deviates from the top of the baffle increases, causing the centrifugal force acting on the

fluid to strengthen accordingly. This effectively promotes fluid disturbance and significantly improves mixing efficiency. Fig. S4d exhibits the *z*-direction velocity distribution at the point of maximum velocity peak under the aforementioned three flow rates. It can be observed that at the vast majority of positions in the *z*-direction of the reactor, the flow velocity has reached the maximum velocity in the *y*-direction and is distributed uniformly and symmetrically.

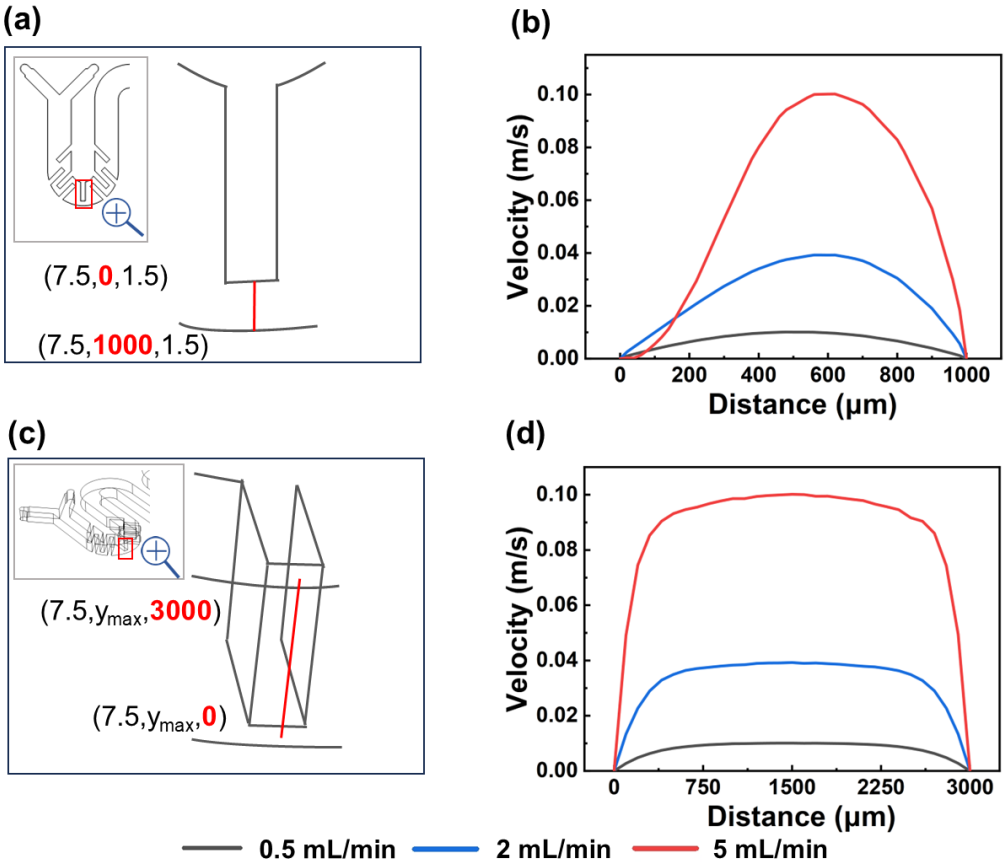

Fig. S4 (a) Three-dimensional coordinates of the baffle in the *y*-direction. (b) Velocity distribution in the *y*-direction of the baffle. (c) Three-dimensional coordinates of the baffle in the *z*-direction. (d) Velocity distribution in the *z*-direction of the baffle.

Experimental Section

1. Materials

Sulfuric acid (AR, 95-98%) and Acetonitrile (AR, ≥99.5%) were purchased from Tianjin Kermel Chemical Reagent Co. Hydrogen peroxide (H_2O_2, 30%) and hydrogen bromide (HBr, 48%) were bought from Shanghai Aladdin Biochemical Technology Co. 1,5-dihydroxy naphthalene (DHN, 98%) was provided by

Beijing Coupling Technology Co. Methyl 2-(methoxyimino)-2-o-tolylacetate (MMOT, 95%) was obtained from Zhengzhou Alpha Chemical Co. 1,2-dichloroethane (AR, ≥99.5%) was bought from Tianjin Damao Chemical Reagent Factory.

2. Homogeneous photochemical reaction

As shown in Fig. S5, the yield of **$M_{3\text{-large}}$** enhances significantly when the flow rate is above 1 mL/min (with the highest yield reaching 100%), with an average increase of 30%. This demonstrates that extending the length of the reactor channel can effectively improve the reaction performance when the flow rate remains constant, meeting the requirements of practical production.

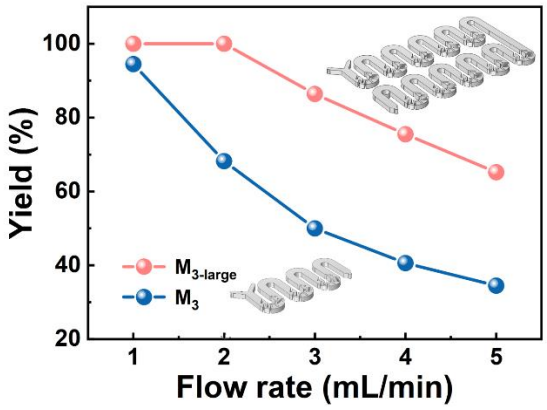

Fig. S5 The dependences of juglone yield on the flow rate in **M_3** and **$M_{3\text{-large}}$**.

The DHN photo-oxidation reaction yield is calculated as follows：

$$\text{Yield}(\%)=\frac{c}{c_0/2}=\frac{2(A_1-A_0)}{Kbc_0}, \quad (2)$$

Where A_0 and A_1 are the absorbances of the mixed solution of DHN and 2I-BDP before and after the reaction at UV absorption wavelength of 403 nm, respectively, K is the molar absorbance coefficient of the reaction product juglone (2640 $M^{-1}\cdot cm^{-1}$), and b is the length of the optical path (1 cm), c_0 is the initial concentration of DHN.

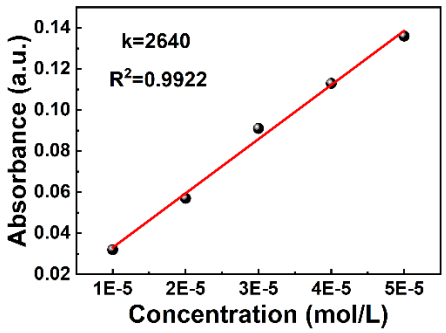

Fig. S6 Determination of the molar absorption coefficient of juglone in acetonitrile solution.

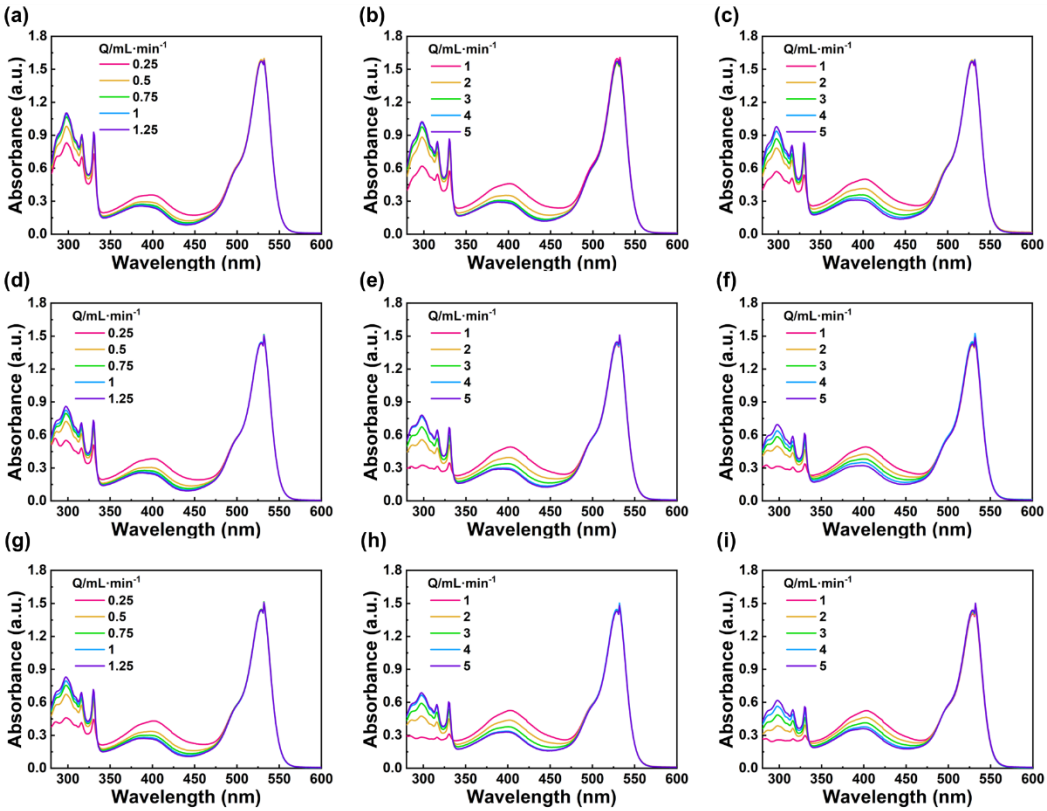

Fig. S7 UV absorption spectra of **M1**-**M3** (from left to right) at different optical power densities: (a-c) 10 mW/cm^2, (d-f) 20 mW/cm^2, (g-i) 30 mW/cm^2.

3. Comparison of M1 and M3 space utilization

When the **M1** and **M3** reactors occupy the same ground area, compared to **M1**, **M3** increases the reactor volume by about 15 times and simultaneously amplifies the flow rate by 12 times, thereby increasing the reaction flux by approximately 180 times, reflecting the high efficiency of spatial utilization and reaction flux advantage of **M3**.

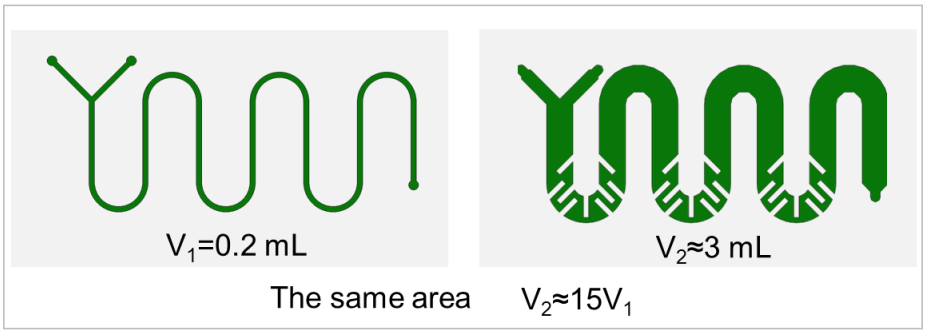

4. The actual reactor photographs of $M_{2\text{-large}}$ and $M_{3\text{-large}}$

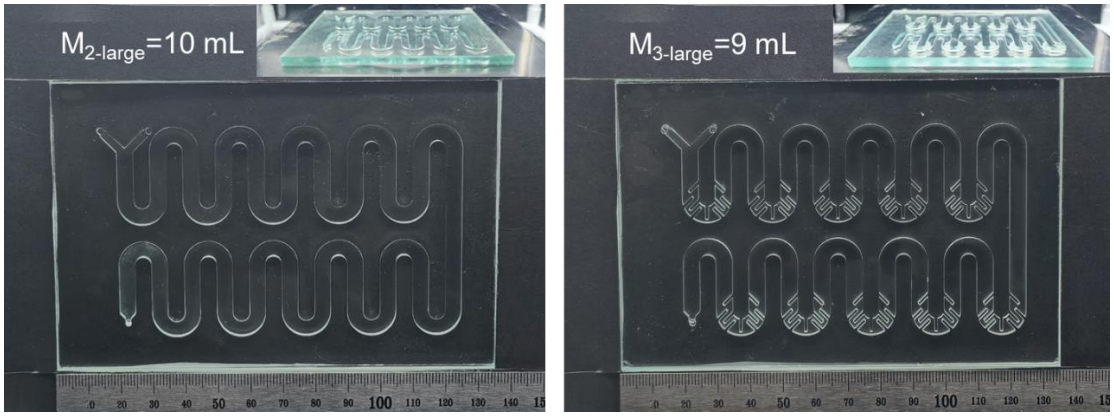

Reference

1. H. Wang, P. Iovenitti, E. Harvey and S. Masood, *Smart Mater. Struct.*, 2002, **11**(5), 662-667.